Competing orbital ordering in RVO(3) compounds

Sage, M. H.; Blake, G. R.; Marquina, C.; Palstra, T. T. M.

Published in:
Physical Review. B: Condensed Matter and Materials Physics

DOI:
10.1103/PhysRevB.76.195102

Publication date:
2007

Competing orbital ordering in RVO_3 compounds: High-resolution x-ray diffraction and thermal expansion

M. H. Sage,[1] G. R. Blake,[1] C. Marquina,[2] and T. T. M. Palstra[1]
[1]*Solid State Chemistry Laboratory, Materials Science Centre, University of Groningen, Nijenborgh 4, 9747 AG Groningen, The Netherlands*
[2]*Instituto de Ciencia de Materiales de Aragón (ICMA), DFMC-ICMA, CSIC-Universidad de Zaragoza, Pedro Cerbuna 12, Zaragoza 50009, Spain*
(Received 4 December 2006; revised manuscript received 20 May 2007; published 1 November 2007)

We report evidence for the phase coexistence of orbital orderings of different symmetry in RVO_3 compounds with intermediate-size rare earths. Through a study by high-resolution x-ray powder diffraction and thermal expansion, we show that the competing orbital orderings are associated with the magnitude of the VO_6 octahedral tilting and magnetic exchange striction in these compounds and that the phase-separated state is stabilized by lattice strains.

DOI: 10.1103/PhysRevB.76.195102 PACS number(s): 61.10.Nz, 61.50.Ks, 71.70.Ej

I. INTRODUCTION

Transition metal oxides with competing interactions have in recent years been shown to exhibit complex electronic behavior, in which different electronic phases may coexist. The competing interactions include spin, charge, and orbital degrees of freedom. The origin of the phase coexistence is often associated with coupling of the electronic degrees of freedom to the lattice. Much interest has been triggered by colossal magnetoresistance materials where a metal-insulator transition involves a discontinuous change in the molar volume.[1–4] Such a first-order transition can lead to phase coexistence of metallic and insulating states, where the length scales of these states are determined by strain and stress. In $(La,Sr)MnO_3$ and $(La,Ca)MnO_3$,[5] such phase coexistence has been observed for low concentrations of the divalent cation as droplets, and it results from competition between the "potential" and "kinetic" energies of the valence electron system. Electron delocalization is promoted by kinetic energy, whereas localization is promoted by the Coulomb repulsion between electrons. In manganite systems, extremely diverse types of phase separation can develop, occurring on a variety of length scales that can range from micrometers down to a few nanometers. Interestingly, phase coexistence not associated with metal-insulator transitions has also been observed; it can arise from competition between different charge-ordered and orbitally ordered or disordered phases.[6,7] Phase separation has also been observed in non-manganite systems, for example, in titanate perovskites, where the coexistence of two phases of different volumes is stabilized by strain.[8,9] Strain-stabilized phase coexistence has also been reported in $LaSrCuO_4$ (Ref. 10) and Ca_2FeRuO_6,[11] as well as in manganites.[12]

The spin, charge, and orbital orderings found in transition metal oxides are often associated with large displacements of the ions in the lattice or even with changes in the molar volume. This gives rise to strains at the interfaces of transformed and untransformed domains, stabilizing the phase coexistence. In the manganites, the orbital and charge orderings generally take place at higher temperatures than the magnetic ordering.[13] In both cases, the coupling between the different phases is mediated through coupling with the lattice. The coupling of orbital and spin orders is mostly of electronic nature by the antisymmetrization requirement of the wave function. In $LaMnO_3$,[14] the orbital interactions between the e_g electrons are much stronger ($T_{OO} \sim 800$ K) than the magnetic interactions ($T_N \sim 150$ K). In contrast, the Jahn-Teller active t_{2g} electrons in the vanadates orbitally order at $T_{OO} \sim 200$ K or lower. The orbital ordering (OO) temperature is always higher than the magnetic ordering temperature with the exception of $LaVO_3$. The type of OO is associated with a particular bonding pattern. In the *C*-type OO, the $d_{xy}d_{yz}$ and $d_{xy}d_{xz}$ orbitals are alternately occupied in the *ab* plane, while the orbital occupation on adjacent V sites along *c* is the same. For each V atom, this gives rise to two short and two long V-O distances in the *ab* plane, a pattern that is "in phase" in adjacent planes along *c* and compatible with *Pbnm* symmetry. However, in the *G*-type OO, where the $d_{xy}d_{yz}$ and $d_{xy}d_{xz}$ orbitals are alternately occupied on adjacent V sites along all three directions, the V-O bonding pattern in successive *ab* planes is arranged "out of phase" (Fig. 1). A detailed

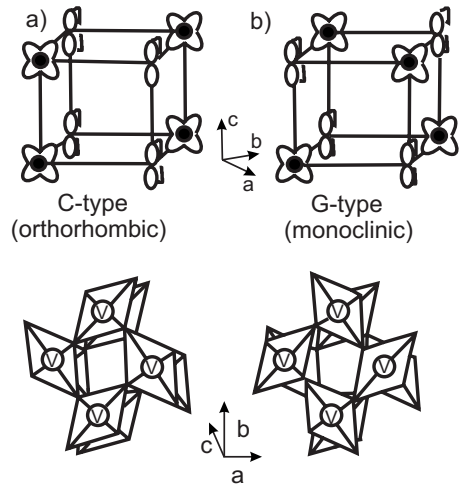

FIG. 1. Schematic picture of the orbital orderings found in RVO_3 compounds (R=rare earth or yttrium) together with associated long and short V-O bonds.

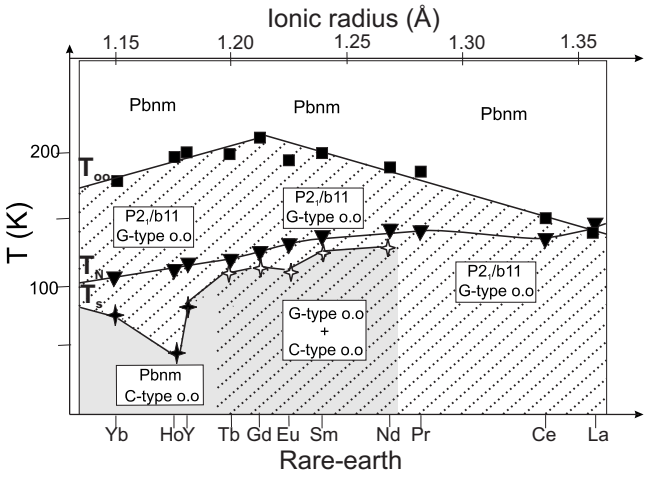

FIG. 2. Phase diagram obtained for RVO_3 studied by diffraction techniques, including data from Refs. 15, 24, 25, and 31. The squares represent the onset of OO, the triangles represent V-spin ordering, filled stars represent the transition from *G*- to *C*-type OO, and open stars represent the transition from *G*-type to coexistence of *G*- and *C*-type OO.

discussion of the structure is given elsewhere.[15]

For RVO_3 with large ionic radius R cations ($r_R > r_{Nd}$), the *G*-type OO (Fig. 1) sets in between 140 and 180 K and remains down to the lowest temperatures. For compounds with small R cations ($r_R < r_{Tb}$), the octahedral tilting is greater and a more complex behavior has been observed:[16,17] the *G*-type OO sets in at $T_{OO} \sim 200$ K, then at a temperature T_s ranging from 50 to 80 K depending on the rare earth, a first-order transition to a *C*-type OO ground state takes place (Fig. 1). In the small-R compounds, the change in the orbital configuration is accompanied by a change in V-spin order. This indicates a strong coupling between the two types of order as required by the antisymmetric nature of the electron wave function, including spin and orbit. Nevertheless, the orders originate at distinctly different temperatures.

We recently reported an unusual phenomenon in the case of $SmVO_3$.[8] We observed a phase coexistence of *G*-type and *C*-type orbital orderings triggered by the antiferromagnetic ordering of the vanadium spins. We attributed this phase coexistence to the intermediate ionic size of samarium, for which the two types of OO have similar energies, and the effect of exchange striction associated with the vanadium spin ordering. This characteristic of $SmVO_3$ led us to propose a phase diagram for the RVO_3 compounds different to that previously reported.[16] We thus decided to perform a similar study on other RVO_3 with intermediate-size rare earths (R=Tb,Gd,Eu,Nd,Pr) in order to verify whether $SmVO_3$ is unique in presenting the phase coexistence of OO. We present here our results showing that the compounds with R=Tb,Gd,Eu,Sm also display a coexistence of *G*- and *C*-type orbital orderings. We show how the competition between the octahedral tilting (more pronounced for smaller rare earths) and the magnetic exchange striction (more pronounced for larger rare earths) is associated with this phenomenon. We present in Fig. 2 a phase diagram for RVO_3 studied by diffraction techniques, which includes results from Refs. 15, 24, 25, and 31.

II. EXPERIMENT

Polycrystalline samples of RVO_3 were prepared by chemical reduction of RVO_4 at 1400 °C under a H_2/N_2 atmosphere. The RVO_4 powders were prepared by solid state reaction, using predried R_2O_3 (99.9% purity) and between a 2% and 10% excess of V_2O_5 (99.95% purity) to compensate for the high volatility of vanadium. Data collected on a laboratory x-ray diffractometer did not contain any impurity peaks, except for the $SmVO_3$ sample which contained a small amount of V_2O_3. High-resolution synchrotron x-ray powder diffraction experiments were carried out on beamline ID31 of the European Synchrotron Radiation Facility (ESRF). The samples were mounted in glass capillaries and data were collected using an x-ray wavelength of 0.4 Å. The powder diffraction patterns were analyzed by the Rietveld method[18] using the refinement program GSAS[19] as implemented in the EXPGUI package.[20] Two types of diffraction experiments were carried out. First, "short scans" were performed for 5–10 min over a limited angular range upon continuous cooling from room temperature to 5 K at a rate of approximately 1 K/min. The resulting data are sufficient for a precise determination of the lattice parameters, cell volume, monoclinic angle, and phase fractions, but they do not allow the determination of the oxygen fractional coordinates. Second, "long scans" were performed for 2–3 h at fixed temperatures, giving data that could be used to determine atomic parameters including oxygen coordinates; these values were used in the analysis of the short scans. Linear thermal expansion (LTE) experiments were performed from liquid He up to room temperature on pressed pellets at the ICMA (CSIC-University of Zaragoza), following a method described previously.[21]

III. RESULTS

A. Compounds with R=Tb,Gd,Eu,Sm

The RVO_3 (R=rare earth or yttrium) compounds all adopt an orthorhombic perovskite structure at room temperature. We could index the high-resolution x-ray diffraction patterns of the RVO_3 compounds (R=Tb,Eu,Gd,Sm) at room temperature with the *Pbnm* space group, an example of which is shown for $GdVO_3$ in Fig. 3 (top panel). Below T_{OO}, the symmetry changes to monoclinic $P2_1/b11$,[22] as evidenced by the splitting of the diffraction lines containing nonzero k and l Miller indices. For some samples, the splitting is poorly resolved and is manifested in the broadening of these diffraction peaks [Fig. 3 (middle panel)]. We identify this change in symmetry with the onset of OO. The monoclinic phase persists from T_{OO} down to the magnetic ordering temperature at T_N. Shortly below T_N, we observe the appearance of additional diffraction peaks corresponding to a second phase, for example, the 132 peak at $d \sim 1.595$ Å in Fig. 3 (lower panel). The b/a lattice parameter ratio of the new phase allows us to assign orthorhombic *Pbnm* symmetry, as described later. We thus have evidence for the coexistence of phases with monoclinic ($P2_1/b11$) and orthorhombic (*Pbnm*) symmetries, which remains down to our lowest measurement temperature of 5 K for all four compounds.

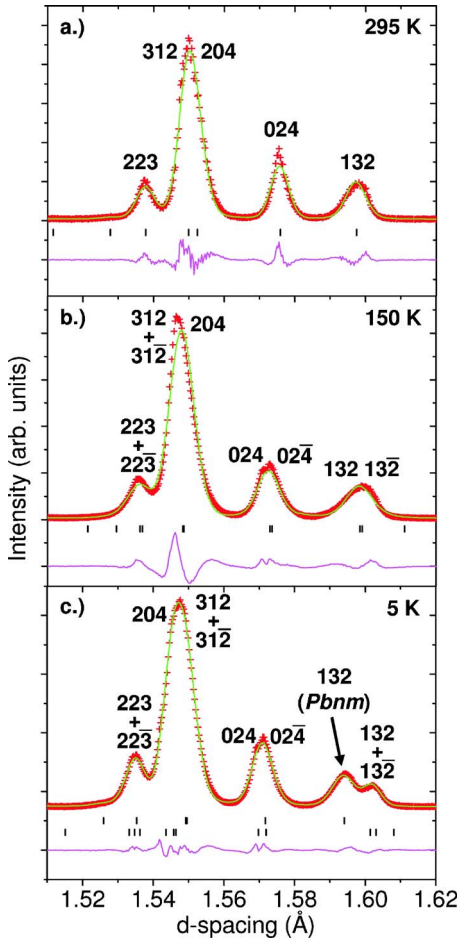

FIG. 3. (Color online) Observed (red crosses), calculated (green line), and difference synchrotron x-ray diffraction patterns of GdVO_3 showing the development of successive phases on cooling: (a) $T > T_{\mathrm{OO}}$, *Pbnm* symmetry, (b) $T_N < T < T_{\mathrm{OO}}$, $P2_1/b11$ symmetry, and (c) $T < T_N$, *Pbnm* (top markers) and $P2_1/b11$ (bottom markers) phases.

The value of the monoclinic angle α increases from 90.00° on cooling through T_{OO}, as shown in Figs. 4(a)–4(e). In the case of TbVO_3, it was difficult to follow the evolution of the monoclinic angle accurately at lower temperatures due to poorly resolved peak splitting. As the rare earth becomes larger, the peak splitting becomes better resolved as the monoclinic angle deviates more from 90° [Figs. 4(a)–4(d)]. As displayed in Fig. 4(f), the proportion of the orthorhombic phase increases rapidly after it first appears, before essentially stabilizing to a final value. In SmVO_3 where data were collected both upon cooling and warming, the evolution of the phase fractions was similar in both cases.[8]

To avoid presenting too many figures, the lattice parameter ratios c/a and b/a, the unit-cell volume, and the LTE for GdVO_3 are shown by way of illustration in Fig. 5, while corresponding data for the other compounds can be consulted in the auxiliary material (EPAPS).[23] The onset of OO is not always accompanied by a change in the unit-cell volume. Although changes in the slope of the volume versus temperature curve were observed for SmVO_3 (Ref. 8) and to a lesser extent EuVO_3, no anomaly is present for GdVO_3 [Fig. 5(b)] and TbVO_3. However, the onset of OO is always accompanied by a change in the lattice parameters and is clearly seen in the c/a ratio (see EPAPS[23]).

The OO transition is also clearly seen by a change in slope of the LTE curve at T_{OO} and in a marked anomaly in the LTE coefficient at this temperature [see Fig. 5(c) for GdVO_3]. The T_{OO} derived from the appearance of these anomalies is in good agreement with previously reported specific heat measurements.[8,16] The LTE coefficient also shows a pronounced anomaly associated with the onset of phase separation [Fig. 5(c) for GdVO_3]. Over the temperature range of 5–300 K, the LTE coefficient is approximately one-third of the volume thermal expansion coefficient calculated from diffraction data [Fig. 5(b)] if the weighted average of the monoclinic and orthorhombic volumes is considered.

The V-O1, V-O2, and V-O3 distances, where O1 are the out-of-plane and O2 and O3 are the in-plane oxygens, are important indicators of the type of OO of a system. In our data they are difficult to determine accurately because there is a considerable overlap of peaks from the two coexisting phases at low temperatures and also because scattering from the heavy rare-earth ions largely dominates the diffraction pattern. We note that when refining the atomic coordinates with a tiny soft constraint (using a weighting factor $F = 0.001$ on the constraint in the GSAS model), very reasonable values for all the V-O distances are obtained. The bond distances and angles determined without using restraints are listed in the EPAPS.[23] Although some individual V-O distances lie outside the expected range of values, taken together they confirm that the RT structure is not orbitally ordered and strongly suggest that at 5 K, both the monoclinic and orthorhombic phases are orbitally ordered. The V-O distances in the monoclinic and orthorhombic phases are generally comparable within error bars to those in the *G*-type and *C*-type OO phases of YVO_3, respectively.[24]

To confirm the nature of these phases over the whole temperature range, we have chosen the lattice parameter ratio b/a [Fig. 5(d), for example, in the case of GdVO_3] as an indicator of the type of OO and compared it to the ratios found for other $R\mathrm{VO}_3$.[8] In $R\mathrm{VO}_3$ compounds where a complete transition from *G*-type (above T_s) to *C*-type (below T_s) OO is observed[8] (i.e., no phase coexistence is found), a discontinuous decrease in the b/a ratio on cooling clearly illustrates the position of T_s. This comparison provides further evidence that the low-temperature orthorhombic phase of GdVO_3, which has a smaller b/a ratio, possesses *C*-type OO. For $R\mathrm{VO}_3$ with small *R*, the transition from *G*- to *C*-type OO occurs at a temperature much lower than T_N.[24,25] In contrast, our results show that for $R\mathrm{VO}_3$ with intermediate *R*, the transition between orbital orderings sets in very close to T_N.

B. Compounds with $R = \mathrm{Nd}, \mathrm{Pr}$

NdVO_3 and PrVO_3 retain their orthorhombic structure down to $T_{\mathrm{OO}} \sim 185$ K. Here, the symmetry changes to monoclinic $P2_1/b11$, as evidenced by the same splitting of diffraction lines as for $R = \mathrm{Tb}, \mathrm{Gd}, \mathrm{Eu}, \mathrm{Sm}$. We identify this change in symmetry with the onset of OO. This is confirmed by other reports[16] and is clearly seen in the c/a ratio (see

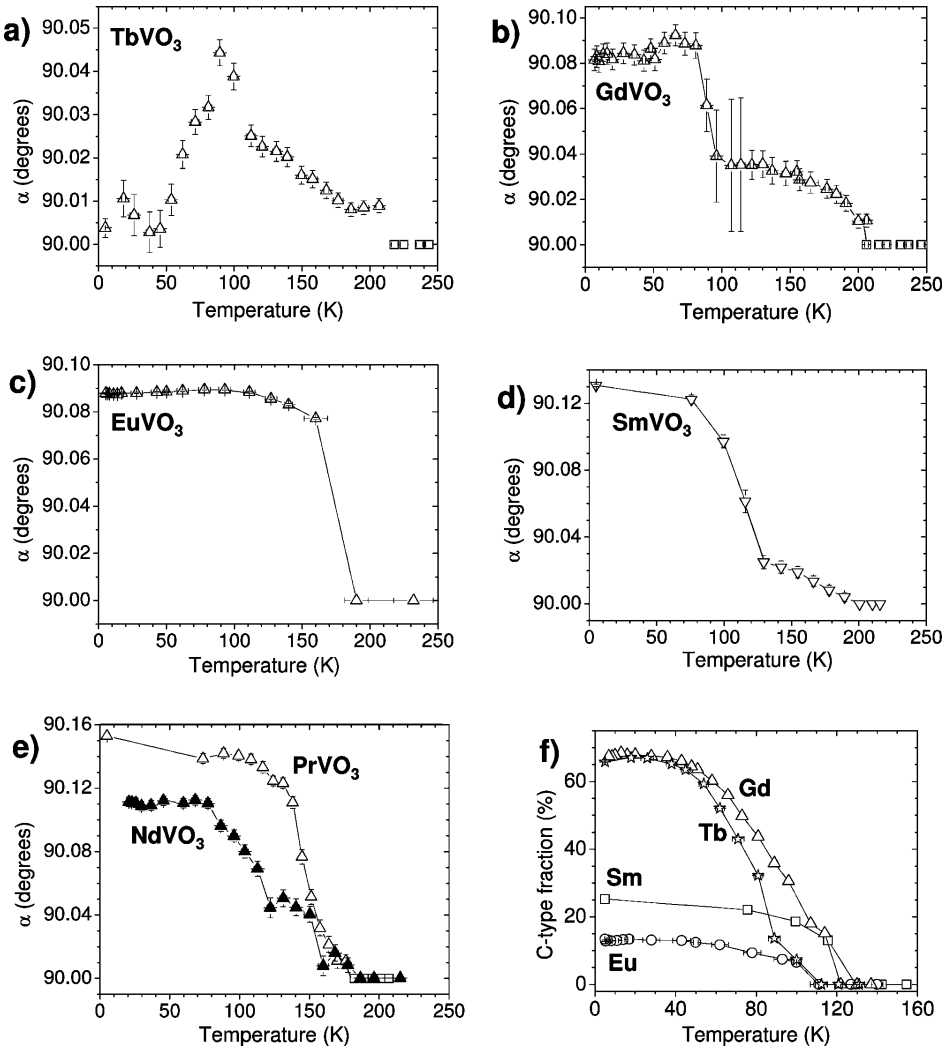

FIG. 4. Temperature dependence of the monoclinic angle, α for (a) $TbVO_3$, (b) $GdVO_3$, (c) $EuVO_3$, (d) $SmVO_3$, (e) $NdVO_3$, and $PrVO_3$. (f) Temperature dependence of the fraction of the C-type OO phase for RVO_3 (R = Tb, Gd, Eu, Sm).

EPAPS[23]). The value of the monoclinic angle increases on cooling and stabilizes shortly below T_N in $PrVO_3$ and below 80 K in $NdVO_3$ [Fig. 4(e)]. The onset of OO is not accompanied by a change in unit-cell volume for either compound. The monoclinic phase persists down to 5 K for both compounds. It should be noted that in the case of $NdVO_3$, there is a hint of a second phase in the 5 K diffraction pattern; we observed intensity above the background level at the position expected for the 020 peak of the C-type phase. However, this was the only C-type peak clearly visible and it would correspond to a phase fraction of the order of 1%, so we are unable to confirm the presence of a C-type OO phase at low temperature. The V-O distances (see EPAPS[23]) provide evidence that the room temperature phase is orbitally disordered and the low-temperature phase is orbitally ordered.

IV. DISCUSSION

The type of OO present in the ground state of the RVO_3 compounds depends mainly on the degree of octahedral tilting caused by the deviation in size of the rare-earth cation from that in the ideal cubic perovskite. The first-order transition from G- to C-type OO for compounds with rare earths of small ionic radius ($r_R < r_{Tb}$) involves a large decrease in the unit-cell volume. In these strongly distorted structures, the C-type ground state is largely stabilized by a shift of the R cation in order to maximize the $R-O$ covalency.[17,26]

It should be pointed out that recent theoretical work predicts the existence of orbital fluctuations in the RVO_3 compounds, especially in the monoclinic phase.[27] However, in order to take this aspect into account, one should perform structural investigations using symmetry lower than $P2_1/b11$. Optical and neutron spectroscopy studies on YVO_3 single crystals have shown that the symmetry of the G-type OO phase is actually lower than $P2_1/b11$, most likely being $Pb11$ or $P\bar{1}$.[28,29] Similar studies on other RVO_3 compounds are required in order to confirm this fact for all members of the series. In our study, we restrict ourselves to space group $P2_1/b11$ as single crystals would be needed for the determination of accurate O positions in models of lower symmetry.

RVO_3 compounds with R of intermediate ionic radius (Tb, Gd, Eu, Sm) have previously been studied mainly by specific heat. As observed in our thermal expansion, high-resolution x-ray diffraction, and specific heat [for $SmVO_3$ (Ref. 8)] measurements, G-type OO develops in this group of RVO_3 near 200 K. It is well known that a structural distor-

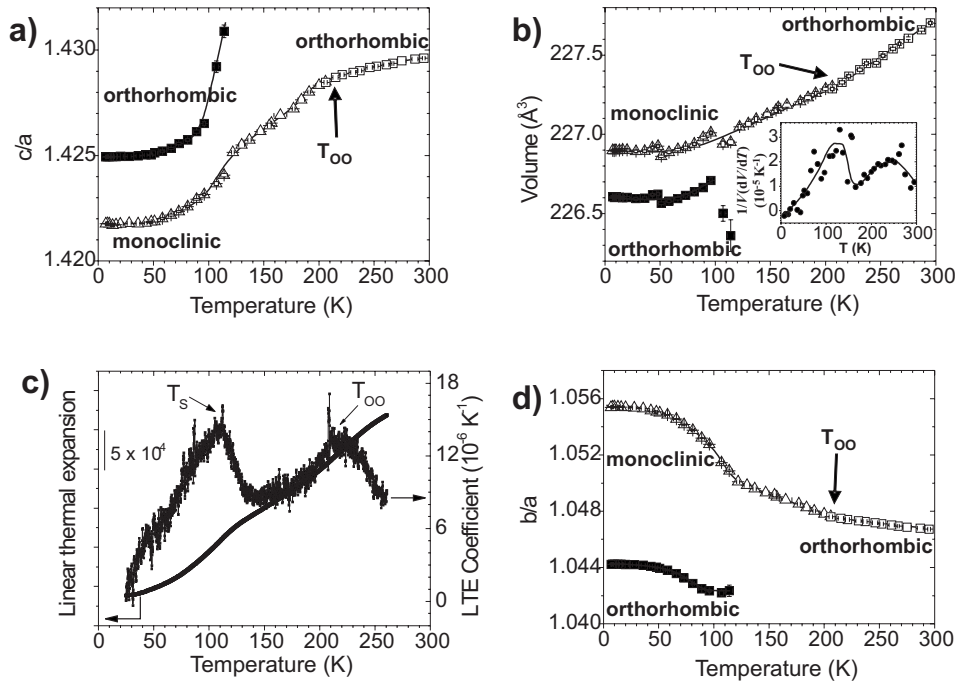

FIG. 5. $GdVO_3$. (a) Temperature dependence of the c/a lattice parameter ratio. (b) Temperature dependence of the volumes of the orthorhombic and monoclinic phases. The inset shows the volume thermal expansion calculated from diffraction data, using a weighted average of the volumes of the monoclinic and orthorhombic phases below T_s; the solid line is a guide to the eyes. (c) Linear thermal expansion (LTE) and temperature dependence of the LTE coefficient. (d) Temperature dependence of the b/a lattice parameter ratio.

tion, known as magnetic exchange striction, can occur at or shortly below T_N in transition metal oxides in order to increase the magnetic exchange interaction energy.[30] This type of distortion has previously been observed in $LaVO_3$ (Refs. 31 and 32) and $CeVO_3$.[31] In the case of $CeVO_3$, the type of OO remains the same below T_N, but the exchange striction occurring at T_N involves a small increase in a and b, a large decrease in c, and an overall decrease in the unit-cell volume. In the case of $LaVO_3$, G-type OO arises 2 K below the magnetic ordering temperature and may itself be triggered by the magnetic ordering transition. However, in the "small radius" RVO_3 compounds such as YVO_3 and $HoVO_3$, the volume change at T_N is negligible,[21,33] indicating that there is little or no exchange striction for small R. The difference between the orbital and magnetic ordering temperatures in these compounds is much larger than in $LaVO_3$ and $CeVO_3$,[16] and V-O bond lengths suggest that OO is fully developed at T_N.[17] Therefore, there is little further energy to be gained through a structural distortion. As previously mentioned, a complete transition to the C-type OO phase is induced at $T_s < T_N$; the degree of octahedral tilting increases slightly on cooling and probably reaches a critical magnitude at T_s, beyond which the C-type OO phase is strongly favored. The change of the dominant phase transition mechanism from "exchange striction induced" to "octahedral tilting induced" between R=Tb and R=Dy, as discussed in detail below, leads to a discontinuous drop in the value of T_s. Taking the specific heat data of Miyasaka *et al.*[16] together with our diffraction studies summarized in Fig. 2, the general trend is for the value of T_s to increase slightly with decreasing r_R beyond R=Dy because the octahedral tilting reaches its critical magnitude at higher temperatures for the smallest rare earths. We note that the value of T_s for R=Y seems to be anomalously high when compared with those for the cations of similar radius, R=Dy and Ho.

The exchange striction occurring at T_N in RVO_3 with R of intermediate ionic radius is expected to be intermediate in magnitude between that in $CeVO_3$ and YVO_3. Since in RVO_3 the exchange striction appears to cause a volume decrease when the temperature is lowered, one may expect the onset of magnetic ordering to promote the C-type phase; that is, the C-type phase will be lowered in energy with respect to the G-type phase to an extent that depends on the magnitude of the exchange striction. For compounds such as $CeVO_3$, the G-type phase is much lower in energy at all temperatures due to the smaller degree of octahedral tilting. At the other end of the phase diagram, the exchange striction in the G-type phase at T_N is too weak to have any effect on the crystal structure. However, for materials closer to the phase boundary such as $SmVO_3$ and $EuVO_3$, the exchange striction is still significant and may be strong enough to lower the energy of the C-type phase enough to become favored. We present a schematic energy diagram of the relative stabilities of the orthorhombic and monoclinic phases for RVO_3 with small (Y), intermediate (Sm), and large ionic radius (Ce) rare earths in Fig. 6. We note that the fraction of the C-type phase for $EuVO_3$ is smaller than that of $SmVO_3$, the opposite of the trend expected when considering the magnitude of the octahedral tilting alone. However, the magnetic exchange striction is weaker in $EuVO_3$ than in $SmVO_3$ and will thus be less of a factor in lowering the energy of the C-type phase. The balance between the influence of octahedral tilting and magnetic exchange striction then results in a C-type phase that is lowered in energy to a slightly smaller extent in $EuVO_3$, giving a smaller phase fraction. We obtain 67% of the C-type phase in both $TbVO_3$ and $GdVO_3$ at 5 K.

The phase separation can be described by a scenario where small droplets of the C-type phase are initially nucleated in a G-type matrix. Although the C-type droplets can be distinguished by x-ray diffraction, they are still relatively small and isolated compared to the surrounding G-type matrix. The unit-cell parameters of regions of a droplet close to an interface will be forced to match those of the surrounding

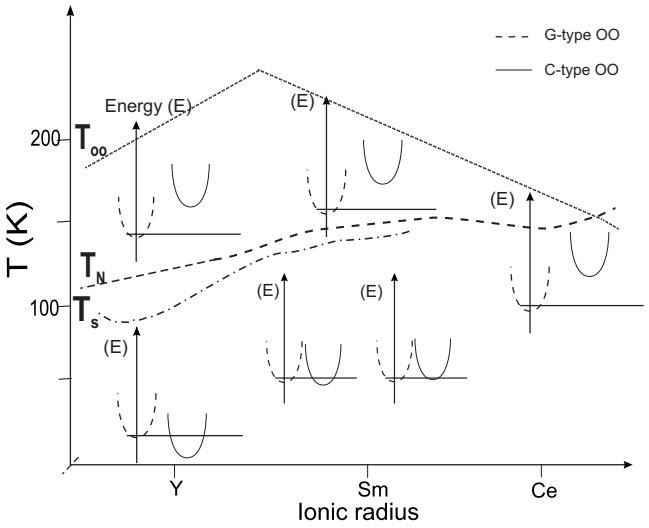

FIG. 6. Schematic diagram for RVO_3 showing relative energies of the *G*- and *C*-type OO phases for small, intermediate, and large ionic radii *R* as a function of temperature.

matrix and large strain fields will thus extend throughout these small droplets. On further cooling, the *C*-type droplets will tend to enlarge and coalesce into domains large enough for relaxation of the strain to take place. This relaxation is seen in the rapid decrease of the unit-cell volume as the fraction of the *C*-type phase grows. However, the remaining strain might still be large enough to inhibit further transformation of the *G*-type matrix, stabilizing the phase-separated state with little change in the phase fractions below ~80 K.

We note that our samples were polycrystalline, and it would be informative to investigate if strain of large enough magnitude develops in single crystal compounds. A recent study of the magnetic structure of $TbVO_3$ single crystals made no mention of phase separation at low temperatures.[34] In addition, the specific heat measurements of the RVO_3 series by Miyasaka *et al.*[16] did not reveal phase coexistence. However, in our $SmVO_3$ sample, the entropy involved at the phase separation temperature is too small to be detected by specific heat and is hidden by the large entropy change exhibited at the spin ordering temperature.[8]

Several features of the crystal structure of RVO_3 compounds provide further insight into the nature of the orbital ordering and phase separation; we now focus in more detail on a number of these aspects and address some of the trends occurring across the RVO_3 series.

A. Temperature dependence of lattice parameters

Concerning the *G*-type OO monoclinic phase at 5 K, the *b* parameter increases with the ionic radius of the rare earth to reach a maximum at *R*=Gd. As the ionic radius of *R* increases further, *b* decreases. Thermal expansion measurements of an YVO_3 single crystal[21] reveal that the onset of *G*-type OO gives rise to an expansion of the *b* lattice parameter on cooling. We find a similar trend for the compounds examined in the present study. The origin of this expansion of *b* can be found when studying the V-O bonding pattern within the *ab* planes of the monoclinic phase. If the long V-O bonds are directed more along the *b* axis, then the short bonds are more along the *a* axis and vice versa. One would then expect no anomalous behavior of either the *a* or *b* lattice parameters if the bonding pattern is exactly out of phase in successive *ab* planes. However, the two *ab* planes are crystallographically inequivalent, and the degree of Jahn-Teller distortion in adjacent planes of YVO_3 was found to be slightly different,[24] giving rise to an overall expansion of the *b* axis (see EPAPS[23]). We can thus conclude that the evolution of *b* is closely related to the development of *G*-type OO. In the *C*-type OO phase, the long bonds are always oriented more along the *a* axis, giving rise to an expansion of this axis on cooling at the *G*-type to *C*-type OO transition.

In the phase-separated temperature region, the temperature dependence of the *C*-type phase fraction reflects the evolution of the lattice parameters. In other words, when the *C*-type fraction no longer changes significantly and an equilibrium has been reached, the lattice parameters also change little with further cooling. In a limited temperature range of up to 20 K between the appearance of the *C*-type phase and the point at which its fraction begins to stabilize, anomalous behavior is sometimes observed in the lattice parameters of both phases, most likely caused by large lattice strains when the *C*-type phase starts to develop.

B. Unit-cell volumes in phase-separated region

For RVO_3 with $r_R < r_{Tb}$, where the octahedral tilting is largest, the first-order transition at T_s involves a full transformation to the *C*-type phase. In these compounds, the unit-cell volume decreases on cooling through the transition as follows: 0.16% in YVO_3,[24] 0.15% in $HoVO_3$, and 0.16% in $YbVO_3$.[8] However, we find that the corresponding differences in unit-cell volumes at 5 K in the phase-separated samples are 0.07% in $SmVO_3$, 0.12% in $EuVO_3$, 0.13% in $GdVO_3$, and 0.12% in $TbVO_3$. In the phase-separated region, the lattice parameters of the *C*-type phase are unable to relax to their single-phase values. The difference in unit-cell volumes of the *C*- and *G*-type phases is thus a good indication of the degree of strain in the sample.

C. Shift of the R^{3+} cation

Covalent bonding between the *R* cation and the O atoms is important in the stabilization of the perovskite structure.[35] For the $GdFeO_3$-type distortion relevant to the RVO_3 series, octahedral tilting causes a shift of the *R* cation from its ideal cubic perovskite position in order to maintain covalent bonding with the oxygen. The degree of octahedral tilting slightly increases on cooling. This results in a progressive shift of the *R* cation with decreasing temperature. It has previously been shown theoretically[26] and experimentally[24] that the *R* cation shifts in the $[\bar{1}10]$ and $[\bar{1}00]$ directions when *G*- and *C*-type OO are present, respectively. The same behavior occurs in our samples, as can be seen in Fig. 7.

D. Evolution of the monoclinic angle

In $LaVO_3$ (monoclinic angle, α=90.125° at 5 K) where the *G*-type OO sets in just below T_N,[31] the monoclinic angle

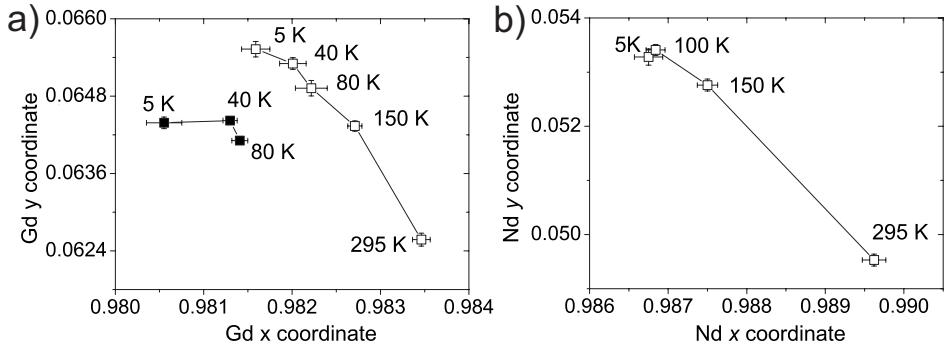

FIG. 7. Variation of rare-earth x and y coordinates with temperature in (a) $GdVO_3$ and (b) $NdVO_3$. Open symbols represent high-temperature and G-type OO phases and closed symbols represent C-type OO phase for $GdVO_3$.

immediately reaches its maximum value. However, for $CeVO_3$ (monoclinic angle, α=90.10° at 5 K) where T_{OO} is slightly higher than T_N, the monoclinic angle gradually increases until it reaches its maximum value at T_N or shortly below.[31] As can be seen in Figs. 4(a)–4(e), similar behavior is observed in $PrVO_3$, $NdVO_3$ and $EuVO_3$, with the slight difference that the maximum value is reached at a temperature coinciding with the onset of the phase separation shortly below T_N in the case of $EuVO_3$ (and possibly $NdVO_3$).

In $SmVO_3$ and $GdVO_3$, the monoclinic angle reaches an essentially constant value on cooling toward T_s, then as the C-type OO phase develops, a sudden increase of the monoclinic angle takes place over a narrow temperature range before another constant value is reached. If the OO of the G-type phase below T_{OO} is not yet complete at T_s, one would expect the monoclinic angle to continue increasing on cooling to 5 K. If the temperature dependence of the monoclinic angle between T_{OO} and T_N is extrapolated to 5 K, one would obtain final values of ~90.04° and ~90.03° for $SmVO_3$ and $GdVO_3$, respectively, at which point the OO should be "complete." However, the sudden jump in the monoclinic angles of $SmVO_3$ and $GdVO_3$ below T_s gives values similar to those of $NdVO_3$ and $PrVO_3$ at low temperature. This suggests that the G-type OO that sets in at T_{OO} is not of exactly the same nature as that found at 5 K and that a transition between the two occurs at T_s. For the compound with the smallest rare earth in our study, $TbVO_3$, the trend of α on cooling is somewhat different; it reaches a maximum value at 90 K and then decreases. The reason for this behavior is unclear, but the "large-α" monoclinic phase that is present at 5 K in all the other samples in this study never develops.

A step in the b lattice parameter below T_s is observed in both $GdVO_3$ and $SmVO_3$ (see EPAPS[23]), close to the point where the monoclinic angle increases. We have discussed above that b is closely correlated with the development of G-type OO. One may thus expect that any change in the nature of the G-type OO would be reflected in the b parameter.

In $NdVO_3$, the rare-earth cation stops shifting with temperature shortly below T_N. At this point, the relatively stable unit-cell parameters suggest that the OO is fully developed. This is supported by the temperature dependence of the monoclinic angle, which reaches a constant value below 85 K. Similar behavior is observed in YVO_3,[17,24] where both bond lengths and the Y shift suggest that the G-type OO is fully developed by T_N. However, the situation in $GdVO_3$ is different, where the rare earth in the G-type OO phase continues to shift with temperature below T_s (Fig. 7). The monoclinic angle also shows a large increase near 85 K. These features may be linked to the development of a different type of G-type OO at low temperature. Unfortunately, the accuracy of our refined O positions is not good enough to pinpoint the difference between the two types of G-type OO phases, which requires further investigation.

E. Summary

We propose a modified phase diagram for the RVO_3 series based on high-resolution x-ray diffraction data (Fig. 2). The type of OO present is influenced by a range of parameters that are dependent on ionic radius, as shown schematically in Fig. 8 and summarized below. The phase diagram between $DyVO_3$ and $LaVO_3$ can be split into two distinct regions. The main characteristics of the first region, for $r_R \leqslant r_{Gd}$, where the octahedral tilting is the dominant factor, are the following.

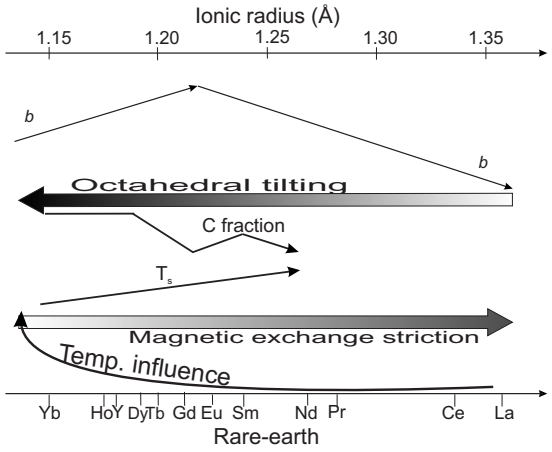

FIG. 8. Ionic radius dependence of parameters influencing the type of orbital ordering: b lattice parameter, magnitude of octahedral tilting, fraction of C-type OO phase, temperature of transition between orbital orderings (T_s), magnitude of magnetic exchange striction, and influence of temperature on inducing the transition between orbital orderings.

(1) T_{OO} increases with ionic radius.

(2) The *G*-type OO phase is favored to T_N or below and the *R* cation in the *G*-type phase shifts approximately along $[\bar{1}10]$ on cooling.

(3) The energy gain from maximizing the *R*-O covalency is very large when *C*-type OO is stabilized below T_s and on cooling, the *R* cation shifts more along the *a* axis in this phase. For *R*=Gd and Tb, the transformation to the *C*-type OO phase is not complete.

(4) The transition from *G*-type to *C*-type OO is mainly temperature induced for smaller rare earths due to the slight increase of octahedral tilting on cooling. A slightly stronger magnetic exchange striction leads to a transformation to *C*-type OO closer to T_N for Tb and Gd compared to smaller *R*: T_s increases with ionic radius.

(5) The monoclinic angle is small ($\sim$90.03°) for $r_R < r_{Gd}$.

The second region of the phase diagram is for $r_R \geqslant r_{Eu}$, where the magnetic exchange striction is the dominant factor:

(1) T_{OO} decreases with increasing ionic radius.

(2) The *G*-type OO phase is favored to T_N and the *R*-O covalency is maximized through a shift of the *R* cation along $[\bar{1}10]$.

(3) For *R*=Eu and Sm (and Nd), magnetic exchange striction lowers the *C*-type OO phase enough in energy to be stabilized in a small fraction of the sample at T_s slightly below T_N, in which the *R* cation shifts more along *a*. T_s increases with ionic radius.

(4) For large *R*, the *G*-type OO phase is favored at all temperatures and phase separation does not occur.

(5) The monoclinic angle is large (90.10°–90.13°) for single-phase *G*-type RVO_3 and small (90.03°) only for $SmVO_3$ above T_s.

V. CONCLUSION

We propose a modified RVO_3 phase diagram in Fig. 2 based on diffraction data. For small rare earths such as Yb, Ho, and Y, complete transformation from *G*-type to *C*-type OO is achieved on cooling through a first-order transition at T_s well below T_N. For large rare earths such as La, Ce, and Pr, the OO remains of *G*-type down to at least 5 K. We show that the border between the *C*- and *G*-type OO phases as a function of ionic radius is not a sharply defined line, as suggested by the phase diagram of Miyasaka *et al.*,[16] but rather occurs via a broad phase-separated region. For intermediate rare earths such as Sm, Eu, Gd, and Tb, a region of coexistence between *C*-type and *G*-type phases is present at all temperatures below T_s close to T_N, where the *C*-type phase fraction increases with the degree of octahedral tilting.

In summary, high-resolution x-ray diffraction, supported by thermal expansion measurements, has demonstrated that octahedral tilting and magnetic exchange striction can both induce a change in symmetry of the OO in part or all of the sample. When the two types of OO are close enough in energy, they can sometimes coexist down to low temperature, a situation that is stabilized purely by strains associated with the difference in lattice parameters of the two phases.

ACKNOWLEDGMENTS

We thank M. Brunelli for experimental assistance at ESRF. We are also grateful to D. I. Khomskii and G. Khaliullin for stimulating discussions. This work was supported in part by the Netherlands Organisation for Scientific Research (NWO).

[1] Y. Tokura and Y. Tomioka, J. Magn. Magn. Mater. **200**, 1 (1999).
[2] E. Dagotto, T. Hotta, and A. Moreo, Phys. Rep. **344**, 1 (2001).
[3] E. L. Nagaev, *Colossal Magnetoresistance and Phase Separation in Magnetic Semiconductors* (Imperial College Press, London, 2002).
[4] C. Sen, G. Alvarez, and E. Dagotto, Phys. Rev. B **70**, 064428 (2004).
[5] J. C. Loudon, N. D. Mathur, and P. A. Midgley, Nature (London) **420**, 797 (2002).
[6] P. G. Radaelli, R. M. Ibberson, D. N. Argyriou, H. Casalta, K. H. Andersen, S.-W. Cheong, and J. F. Mitchell, Phys. Rev. B **63**, 172419 (2001).
[7] J. P. Chapman, J. P. Attfield, L. M. Rodriguez-Martinez, L. Lezama, and T. Rojo, J. Chem. Soc. Dalton Trans. **2004**, 3026.
[8] M. H. Sage, G. R. Blake, G. J. Nieuwenhuys, and T. T. M. Palstra, Phys. Rev. Lett. **96**, 036401 (2006).
[9] K. Kato, E. Nishibori, M. Takata, M. Sakata, T. Nakano, K. Uchihira, M. Tsubota, F. Iga, and T. Takabatake, J. Phys. Soc. Jpn. **71**, 2082 (2002).
[10] Y. Horibe, Y. Inoue, and Y. Koyama, Phys. Rev. B **61**, 11922 (2000).
[11] E. Granado, Q. Huang, J. W. Lynn, J. Gopalakrishnan, R. L. Greene, and K. Ramesha, Phys. Rev. B **66**, 064409 (2002).
[12] A. Machida, Y. Moritomo, E. Nishibori, M. Takata, M. Sakata, K. Ohoyama, S. Mori, N. Yamamoto, and A. Nakamura, Phys. Rev. B **62**, 3883 (2000).
[13] Y. Murakami *et al.*, Jpn. J. Appl. Phys., Part 1 **38**, 360 (1999).
[14] Y. Murakami *et al.*, Phys. Rev. Lett. **81**, 582 (1998).
[15] M. H. Sage, Ph.D. thesis, University of Groningen, 2006.
[16] S. Miyasaka, Y. Okimoto, M. Iwama, and Y. Tokura, Phys. Rev. B **68**, 100406(R) (2003).
[17] G. R. Blake, T. T. M. Palstra, Y. Ren, A. A. Nugroho, and A. A. Menovsky, Phys. Rev. Lett. **87**, 245501 (2001).
[18] H. Rietveld, J. Appl. Crystallogr. **2**, 65 (1969).
[19] A. C. Larson and R. B. von Dreele, Los Alamos Laboratory Report No. LAUR 86–748, 2004 (unpublished).
[20] B. H. Toby, J. Appl. Crystallogr. **34**, 210 (2001).
[21] C. Marquina, M. Sikora, M. R. Ibarra, A. A. Nugroho, and T. T. M. Palstra, J. Magn. Magn. Mater. **290-291**, 428 (2005).
[22] We use $P2_1/b11$ for the monoclinic phase instead of the standard setting $P2_1/c$ in order to allow a direct comparison of the lattice parameters, Miller indices, and atomic coordinates of the mono-

clinic phase with those of the orthorhombic *Pbnm* phase. The monoclinic angle in this setting is α.

[23] See EPAPS Document No. E-PRBMDO-76-080739 for additional structural data. For more information on EPAPS, see http://www.aip.org/pubservs/epaps.html.

[24] G. R. Blake, T. T. M. Palstra, Y. Ren, A. A. Nugroho, and A. A. Menovsky, Phys. Rev. B **65**, 174112 (2002).

[25] G. R. Blake (unpublished).

[26] T. Mizokawa, D. I. Khomskii, and G. A. Sawatzky, Phys. Rev. B **60**, 7309 (1999).

[27] G. Khaliullin, Prog. Theor. Phys. Suppl. **160**, 155 (2005).

[28] A. A. Tsvetkov, F. P. Mena, P. H. M. van Loosdrecht, D. van der Marel, Y. Ren, A. A. Nugroho, A. A. Menovsky, I. S. Elfimov, and G. A. Sawatzky, Phys. Rev. B **69**, 075110 (2004).

[29] C. Ulrich, G. Khaliullin, J. Sirker, M. Reehuis, M. Ohl, S. Miyasaka, Y. Tokura, and B. Keimer, Phys. Rev. Lett. **91**, 257202 (2003).

[30] S. Greenwald and J. S. Smart, Nature (London) **166**, 523 (1950).

[31] Y. Ren, A. A. Nugroho, A. A. Menovsky, J. Strempfer, U. Rütt, F. Iga, T. Takabatake, and C. W. Kimball, Phys. Rev. B **67**, 014107 (2003).

[32] P. Bordet, C. Chaillout, M. Marezio, Q. Huang, A. Santoro, S.-W. Cheong, H. Takagi, C. S. Oglesby, and B. Batlogg, J. Solid State Chem. **106**, 253 (1993).

[33] M. Sikora, C. Marquina, M. R. Ibarra, A. A. Nugroho, and T. T. M. Palstra, J. Magn. Magn. Mater. **316**, e692 (2007).

[34] M. Reehuis, C. Ulrich, P. Pattison, B. Ouladdiaf, M. C. Rheinstädter, M. Ohl, L. P. Regnault, M. Miyasaka, Y. Tokura, and B. Keimer, Phys. Rev. B **73**, 094440 (2006).

[35] J. B. Goodenough and J. M. Longo, in *Crystallographic and Magnetic Properties of Perovskite and Related Compounds*, Landolt-Börnstein Tabellen New Series, Group III, Vol. 4, Pt. A, edited by K. H. Hellwege (Springer-Verlag, Berlin, 1970), pp. 126–314.